Fluid Dynamics & Materials Processing

Tech Science Press

DOI: 10.32604/fdmp.2022.022002

ARTICLE

Analysis of a Stagnation Point Flow with Hybrid Nanoparticles over a Porous Medium

U. S. Mahabaleshwar[1], T. Anusha[1] and M. Hatami[2,*]

[1]Department of Mathematics, Davangere University, Shivagangothri, Davangere, India

[2]Department of Mechanical Engineering, Ferdowsi University of Mashhad, Mashhad, Iran

*Corresponding Author: M. Hatami. Email: m-hatami@um.ac.ir; m.hatami2010@gmail.com

Received: 16 February 2022 Accepted: 25 April 2022

ABSTRACT

The unsteady stagnation-point flow of a hybrid nanofluid over a stretching/shrinking sheet embedded in a porous medium with mass transpiration and chemical reactions is considered. The momentum and mass transfer problems are combined to form a system of partial differential equations, which is converted into a set of ordinary differential equations via similarity transformation. These ordinary differential equations are solved analytically to obtain the solution for velocity and concentration profiles in exponential and hypergeometric forms, respectively. The concentration profile is obtained for four different cases namely constant wall concentration, uniform mass flux, general power law wall concentration and general power law mass flux. The effect of different physical parameters such as Darcy number (Da^{-1}), mass transpiration parameter (V_C), stretching/shrinking parameter (d), chemical reaction parameter (β) and Schmidt number (Sc) on velocity and concentration profile is examined. Results show that, the axial velocity will decreases as the shrinking sheet parameter increases, regardless of whether the suction or injection case is examined. The concentration decreases with an increase in the shrinking sheet parameter and the chemical reaction rate parameter.

KEYWORDS

Chemical reaction parameter; mass transpiration; hybrid nanofluid; porous medium; Schmidt number

Nomenclature

b	Constants $(-)$
C	Concentration field (mol/m^3)
D_B	Molecular diffusivity (m^2s^{-1})
Da^{-1}	Inverse Darcy number $(-)$
k_C	Chemical reaction parameter $(-)$
K	Permeability of porous medium (m^2)
P	Pressure (Nm^{-2})
Sc	Schmidt number $(-)$
V_C	Suction/injection parameter $(-)$
V_w	Mass transfer velocity (ms^{-1})
(u, v)	Velocities along (x, y) direction (ms^{-1})
(x, y)	Cartesian coordinates (m)

Greek symbols

β	Chemical reaction parameter $(-)$
η	Similarity variable $(-)$
μ	Dynamic viscosity $(kgm^{-1}S^{-1})$
v	Kinematic viscosity (m^2s^{-1})
ρ	Density (kgm^{-3})

Subscripts

hnf	Hybrid nanofluid parameter $(-)$
w	Wall condition $(-)$
∞	Ambient condition $(-)$

Abbreviations

HNF	Hybrid nanofluid $(-)$
MHD	Magneto hydrodynamics $(-)$
ODEs	Ordinary differential equations $(-)$
PDEs	Partial differential equations $(-)$
PST	Prescribed surface temperature $(-)$
PHF	Prescribed heat flux $(-)$

Highlights

- This work investigates the unsteady stagnation point flow and mass transfer with chemical reaction.
- The system of partial differential equations is converted into system of ordinary differential equations via similarity transformations.
- The concentration profile is obtained for cases such as constant wall concentration, uniform mass flux, general power law wall concentration and general power law mass flux.
- The axial velocity decreases as the shrinking sheet parameter increases.

1 Introduction

The mass transfer and momentum boundary layer flow have practical interest in the field of polymer process and electrochemistry. Also, the hybrid nanofluid (HNF) flow is a significant field in industry and become an interest field for researchers due to its wide applications. There are many significances of heat transfer over stretching sheet, due to its advantages mentioned by many researchers [1,2]. Aly et al. [3,4] made a comparison between the significances of HNF over NF for the magneto-hydrodynamic (MHD) flow and heat transfer by considering the effect of partial slip. Turkyilmazoglu [5] found the multiple solutions for MHD slip flow of viscoelastic fluid and Anusha et al. [6,7] investigated the unsteady inclined MHD flow for Casson fluid with hybrid nanoparticles in a porous media. Also, Mahabaleshwar et al. [8] investigated the MHD flow behaviour and mass transfer due to porous media. Fang et al. [9] examined the unsteady stagnation point flow and heat transfer to obtain the closed form solutions for prescribed wall temperature and wall heat flux. Mahabaleshwar et al. [10,11] made a research on the MHD flow with carbon nanotubes by considering the effect of mass transpiration and radiation on it. Suresh et al. [12,13] investigated the effect of hybrid nanofluid on heat transfer characteristics and observed that a hybrid nanofluid of (Al_2O_3-Cu/H_2O) had significant heat transfer. Momin [14] investigated the laminar flow in an elevated funnel using mixed convection with a (Al_2O_3-Cu/H_2O) hybrid nanofluid. Recently, the mixed convective flow with radiation is studied by Patil et al. [15] considering the couple stress fluid flow for first order chemical reaction. Furthermore, Mahabaleshwar et al. [16] examined the MHD non-Newtonian fluid flow and heat transfer due to porous surface with

heat source/sink by different solution methods. Mahabaleshwar et al. [17] investigated the steady flow with HNF with mass suction, mathematically, and found the solution in algebraic decaying form. Nakhchi et al. [18,19] studied the effect of CuO-water nanofluid on the improvement of entropy production for a double pipe heat exchanger and a double V-cut twisted tapes, respectively. Recently many works are done on HNF flow by researchers such as Zainal et al. [20] on MHD flow due to quadratic stretching/shrinking sheet, Umair et al. [21] on radiative mixed convective flow, more recent developments and applications of HNF are investigated by Sarkar et al. [22], Vishalakshi et al. [23] studied the effect of slips and mass transpiration on the flow over porous sheet and Sneha et al. [24] on dusty HNF. The effect of nanoparticles on the flow is also investigated by Jalali et al. [25] and Bhandari [26].

Motivated by these investigations, the current work investigates the unsteady stagnation point flow of $Cu\text{-}Al_2O_3/H_2O$ HNF over stretching/shrinking sheet embedded in porous media considering mass transpiration and mass transfer with chemical reaction. The present work has many applications related to heating and cooling processes at high temperature ranges. So, HNF has wide applications in heating and cooling systems, refrigeration, space, machining, manufacturing, and etc. Also, the porous media is used to achieve the applications in thermal energy storage, geothermal recovery, grain storage, electrochemical process, flow through filtering device and chemical catalytic reactors. So, the momentum and mass transfer problems were solved analytically to find a solution of velocity and concentration profiles in exponential and hypergeometric forms, respectively. The concentration profile is obtained for four different cases such as constant wall concentration, uniform mass flux, general power law wall concentration and general power law mass flux. These solutions give a rare case of closed form solutions which can be adapted to some other standard problems. The results have well agreement with the work of Fang et al. [9]. The effects of different physical parameters like Darcy number, mass transpiration parameter, stretching/shrinking parameter, and chemical reaction parameter, Schmidt number on velocity and concentration profiles are examined under different situations.

2 Physical Model

The incompressible unsteady stagnation point flow over stretching/shrinking sheet is embedded in porous media with mass transpiration and mass transfer with chemical reaction as shown in Fig. 1. The $Cu\text{-}Al_2O_3/H_2O$ HNF is used as the main fluid flow. The wall and free stream are moving along x-axis with velocity $U_w = dax(1-\gamma t)^{-1}$ and $U_\infty = ax(1-\gamma t)^{-1}$, respectively and y-axis is perpendicular to it. At the wall; the concentration is maintained constant at C_w with a uniform mass flux $m_w(1-\gamma t)^{-1/2}$ and the concentration of free stream is kept constant at C_∞. The governing 2D continuity, momentum and mass equations are as follows (see Anusha et al. [7], Mahabaleshwar et al. [8]).

$$\frac{\partial u}{\partial x}+\frac{\partial \mathrm{v}}{\partial y}=0, \tag{1}$$

$$\frac{\partial u}{\partial t}+u\frac{\partial u}{\partial x}+\mathrm{v}\frac{\partial u}{\partial y}=-\frac{1}{\rho_{hnf}}\frac{\partial P}{\partial x}+\nu_{hnf}\left(\frac{\partial^2 u}{\partial x^2}+\frac{\partial^2 u}{\partial y^2}\right)+\frac{\nu_{hnf}}{K}(U_\infty-u), \tag{2}$$

$$\frac{\partial \mathrm{v}}{\partial t}+u\frac{\partial \mathrm{v}}{\partial x}+\mathrm{v}\frac{\partial \mathrm{v}}{\partial y}=-\frac{1}{\rho_{hnf}}\frac{\partial P}{\partial y}+\nu_{hnf}\left(\frac{\partial^2 \mathrm{v}}{\partial x^2}+\frac{\partial^2 \mathrm{v}}{\partial y^2}\right), \tag{3}$$

$$\frac{\partial C}{\partial t}+u\frac{\partial C}{\partial x}+v\frac{\partial C}{\partial y}=D_B\frac{\partial^2 C}{\partial y^2}-k_C(C-C_\infty), \tag{4}$$

and the boundary conditions (B.Cs) are,

$$u(x,0,t) = u_w = \frac{dax}{(1-\gamma t)}, \mathrm{v}(x,0,t) = V_w(x,t), C(x,0,t) = C_w(x,t), \tag{5}$$

$$u(x,\infty,t) = u_\infty = \frac{ax}{(1-\gamma t)}, C(x,\infty,t) = C_\infty. \tag{6}$$

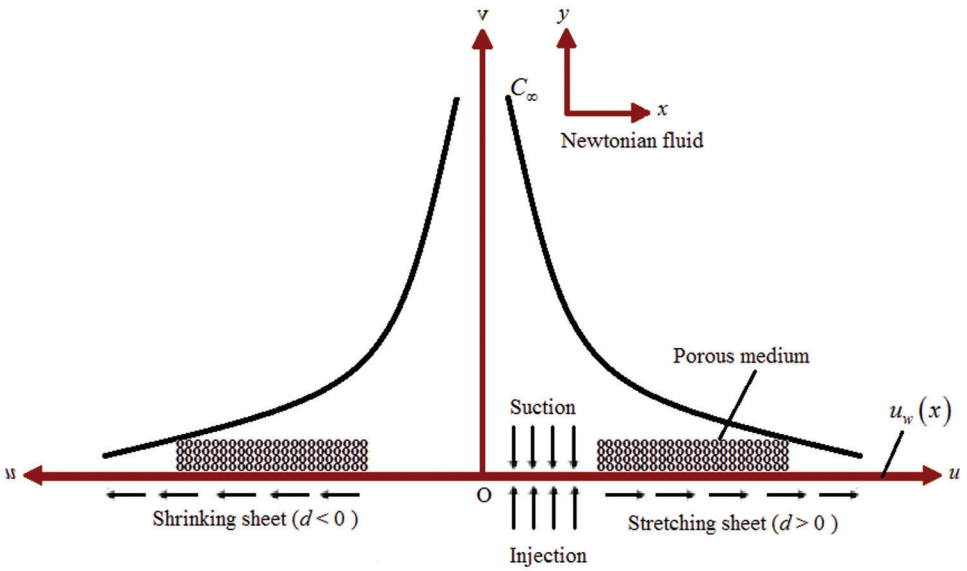

Figure 1: Schematic diagram of the problem

The following similarity transformation is introduced (see Fang et al. [9]) to transform the system of PDEs (1) to (4) into system of ODEs in order to find out the analytical solution,

$$\psi(x,y,t) = ax\sqrt{\frac{\nu_f}{(1-\gamma t)}} f(\eta), \quad \phi(\eta) = \frac{C - C_\infty}{C_w - C_\infty}, \text{ where } \eta = \frac{y}{\sqrt{\nu_f(1-\gamma t)}}. \tag{7}$$

And therefore the velocities along x- and y-axes are obtained as,

$$u = \frac{ax}{(1-\gamma t)} f_\eta(\eta), \quad \mathrm{v} = -a\sqrt{\frac{\nu_f}{(1-\gamma t)}} f(\eta), \tag{8}$$

and wall mass transpiration velocity is,

$$V_w(x,t) = V_w(t) = -a\sqrt{\frac{\nu_f}{(1-\gamma t)}} f(0). \tag{9}$$

On applying x-momentum with $u = u_\infty$ to Eq. (2) we can obtain,

$$-\frac{1}{\rho_{hnf}}\frac{\partial P}{\partial x} = \frac{ax}{(1-\gamma t)^2}(\gamma + a), \tag{10}$$

Use Eqs. (7), (8) and (10) in Eqs. (2) and (4) to get,

$$\delta f_{\eta\eta\eta} + \left(af + \frac{\eta\gamma}{2}\right) f_{\eta\eta} - \left(\gamma + af_{\eta}\right) f_{\eta} + \gamma + a - a\delta Da^{-1}\left(1 - f_{\eta}\right) = 0, \tag{11}$$

$$\phi_{\eta\eta} + Sc\left(af - \gamma\frac{\eta}{2}\right)\phi_{\eta} + aSc\beta\phi = 0, \tag{12}$$

The B.Cs associated with this Eqs. (5) and (6) also reduced as

$$f(0) = V_C \ , \ f_{\eta}(0) = d \ , \ f_{\eta}(\infty) = 1. \tag{13}$$

$$\phi(0) = 1 \ , \ \phi(\infty) = 0, \tag{14}$$

here, $V_C = -\dfrac{V_w(x,t)}{a\sqrt{v_f/(1-\gamma t)}}$ is the mass transpiration parameter, where it is depend on sign of the constant a, i.e., if $a > 0$, then a positive V_C indicates mass suction and negative V_C indicates mass injection, and reversely if $a < 0$, positive V_C indicates mass injection and negative V_C indicates mass suction. $d = \dfrac{u_w}{u_\infty}$ is the wall moving parameter, here also if $a > 0$, positive d indicates the stretching wall and the negative d indicates shrinking wall and if $a < 0$, positive d indicates the shrinking wall and the negative d indicates stretching wall.

Also, $Sc = \dfrac{v_f}{D_B}$ is Schmidt number, $\beta = \dfrac{k_C}{a(1-\gamma t)}$ is chemical reaction parameter, and the quantity $\delta = \dfrac{\delta_2}{\delta_1}$. Further the values and relations are as mentioned in the Table 1.

Table 1: Physical properties of hybrid nanofluid with relations

Physical properties	Base fluid (f) water(H_2O)	Nanoparticles		Relation
		$Al_2O_3(s_1)$	$Cu(s_2)$	
$\rho\ (kg/m^3)$	997.1	3970	8933	$\delta_1 = \dfrac{\rho_{hnf}}{\rho_f} = (1-\phi_2)\left(1 - \phi_1 + \phi_1\dfrac{\rho_{s_1}}{\rho_f}\right) + \phi_2\dfrac{\rho_{s_2}}{\rho_f}$
$\mu(Pas)$	0.96×10^{-3}	–	–	$\delta_2 = \dfrac{\mu_{hnf}}{\mu_f} = \dfrac{1}{(1-\phi_1)^{2.5}(1-\phi_2)^{2.5}}$

2.1 Solution of Pressure Term

Since $\mathrm{v} = \mathrm{v}(y,t)$ Eq. (3) will give,

$$-\frac{1}{\delta_1\rho_f}\frac{\partial P}{\partial y} = \frac{\partial \mathrm{v}}{\partial t} + \mathrm{v}\frac{\partial \mathrm{v}}{\partial y} - \frac{\delta_2}{\delta_1}v_f\frac{\partial^2 \mathrm{v}}{\partial y^2}, \tag{15}$$

and

$\dfrac{\partial P}{\partial y} = g(t,y)$ will give,

$$P = \int g(t,y) + h(t,x), \tag{16}$$

where, $h(t,x)$ is the constant function of the integration respect to y.

$\frac{\partial P}{\partial x}$ On differentiate Eq. (16) w.r.t x to obtain equation as $\frac{\partial P}{\partial x} = \frac{\partial h(t,x)}{\partial x}$, this is free from y. From Eq. (10), $\frac{\partial P}{\partial x}$ can be rewrite as,

$$-\frac{1}{\delta_1 \rho_f}\frac{\partial P}{\partial x} = \frac{ax}{(1-\gamma t)^2}(\gamma + a), \tag{17}$$

The pressure P can be obtained from Eqs. (15) and (17),

$$\frac{1}{\rho_f}(P_0 - P) = \frac{\delta_1 a x^2}{2(1-\gamma t)^2}(\gamma + a), \tag{18}$$

where, P_0 is constant of integration. Integrate Eq. (15) to get,

$$\frac{1}{\rho_f}(P_0 - P) = \delta_1 \int_0^y \frac{\partial \mathrm{v}}{\partial t} dy + \delta_1 \frac{\mathrm{v}^2}{2} - \delta_2 v_f \frac{\partial \mathrm{v}}{\partial y}, \tag{19}$$

From Eqs. (18) and (19),

$$\frac{1}{\rho_f}(P_0 - P) = \frac{\delta_1 a x^2}{2(1-\gamma t)^2}(\gamma + a) + \delta_1 \int_0^y \frac{\partial \mathrm{v}}{\partial t} dy + \delta_1 \frac{\mathrm{v}^2}{2} - \delta_2 v_f \frac{\partial \mathrm{v}}{\partial y}, \tag{20}$$

2.2 Solution for Velocity

Consider a special case with $a = -1/2, \gamma = -1$, then Eq. (11) will give the following form,

$$\delta f_{\eta\eta\eta} - \frac{1}{2}(f - \eta) f_{\eta\eta} + \left(1 + f_\eta\right) f_\eta - \frac{3}{2} + \delta \frac{1}{2} Da^{-1}\left(1 - f_\eta\right) = 0, \tag{21}$$

Defining a new transformation $F(\eta) = f(\eta) - \eta$, and using this in Eq. (21) will give,

$$\delta F_{\eta\eta\eta} - \frac{1}{2} F F_{\eta\eta} + 2F_\eta + \frac{1}{2} {F_\eta}^2 + \frac{1}{2}\delta Da^{-1} F_\eta = 0, \tag{22}$$

And the associated B.Cs will reduces as,

$$F(0) = V_C, \quad F_\eta(0) = d - 1, \quad F_\eta(\infty) = 0. \tag{23}$$

Assume the solution of Eq. (22) is in the form,

$$F(\eta) = c_1 + c_2 Exp(-\alpha\eta). \tag{24}$$

On applying B.Cs defined in Eq. (23),

$$c_1 = V_C + \frac{1-d}{\alpha}, \; c_2 = \frac{1-d}{\alpha}, \tag{25}$$

And on using Eqs. (24) and (25) in Eq. (22) will give,

$$2\delta\alpha^2 + \left(V_C + Da^{-1}\right)\alpha + d + 3 = 0, \tag{26}$$

Its roots will obtained as,

$$\alpha = \frac{-(V_C + Da^{-1}) + \sqrt{(V_C + Da^{-1})^2 - 8\delta(d+3)}}{4\delta}, \tag{27}$$

here, to obtain physically feasible solution Eq. (27) must satisfy $(V_C + Da^{-1})^2 - 8\delta(d+3) \geq 0$. And Eq. (26) will give,

$$V_C = -2\delta\alpha - Da^{-1} - \frac{(d+3)}{\alpha} = 0, \tag{28}$$

The solution will become,

$$f(\eta) = \eta + V_C - \frac{1-d}{\alpha}(1 - Exp[-\alpha\eta]), \tag{29}$$

And axial velocity is given by

$$f_\eta(\eta) = 1 - (1-d)Exp[-\alpha\eta], \tag{30}$$

2.3 Solution for Concentration

For the special case $a = -1/2, \gamma = -1$, the Eq. (12) got the form,

$$\phi_{\eta\eta} - \frac{1}{2}Sc(f-\eta)\phi_\eta - \frac{1}{2}Sc\beta\phi = 0, \tag{31a}$$

Use Eq. (29) in above,

$$\phi_{\eta\eta} - \frac{Sc}{2}\left[V_C - \frac{1-d}{\alpha} + \frac{1-d}{\alpha}Exp(-\alpha\eta)\right]\phi_\eta - \frac{1}{2}Sc\beta\phi = 0, \tag{31b}$$

Then use Eq. (28) in above,

$$\phi_{\eta\eta} + Sc\left[\delta\alpha + \frac{Da^{-1}}{2} + \frac{2}{\alpha} + \frac{d-1}{2\alpha}Exp(-\alpha\eta)\right]\phi_\eta - \frac{1}{2}Sc\beta\phi = 0, \tag{32}$$

On introducing the new variable $\varepsilon = (1-d)\dfrac{Sc}{2\alpha^2}Exp(-\alpha\eta)$ in the Eq. (32) will yield,

$$\varepsilon\frac{\partial^2\phi}{\partial\varepsilon^2} + \left[1 - Sc\left(\delta + \frac{Da^{-1}}{2\alpha} + \frac{2}{\alpha^2}\right) + \varepsilon\right]\frac{\partial\phi}{\partial\varepsilon} - \frac{Sc}{2\alpha^2\varepsilon}\beta\phi = 0, \tag{33}$$

And the B.Cs in terms of new variable are,

$$\phi\left(\frac{Sc(1-d)}{2\alpha^2}\right) = 1, \quad \phi(0) = 0. \tag{34}$$

Then the general solution of Eq. (33) in terms of ε is obtained as,

$$\phi(\varepsilon) = C_1{}^1\varepsilon^{C_1}H[C_1, D+1, -\varepsilon], \tag{35}$$

And Eq. (35) in terms of η will be in the form,

$$\phi(\eta) = {C_1}^1(1-d)^{C_1}\left(\frac{Sc}{2\alpha^2}\right)^{C_1} Exp(-C_1\alpha\eta)H\left[C_1, D+1, (d-1)\frac{Sc}{2\alpha^2}Exp(-\alpha\eta)\right], \tag{36}$$

To obtain value of constant ${C_1}^1$, the B.C in Eq. (14) is used in Eq. (36), the general solution will be,

$$\phi(\eta) = Exp(-C_1\alpha\eta)\frac{H\left[C_1, D+1, (d-1)\frac{Sc}{2\alpha^2}Exp(-\alpha\eta)\right]}{H\left[C_1, D+1, (d-1)\frac{Sc}{2\alpha^2}\right]}, \tag{37}$$

where, $C_1 = \frac{A+D}{2}$, $D = \sqrt{A^2+4B}$, and here

$$A = Sc\left(\delta + \frac{Da^{-1}}{2\alpha} + \frac{2}{\alpha^2}\right) \ , \ B = \frac{Sc\beta}{2\alpha^2} \tag{38}$$

then wall mass flux is given by,

$$-\phi_\eta(0) = \frac{Sc(1-d)}{2\alpha}\frac{C_1}{D+1}\frac{H\left[C_1+1, D+2, (d-1)\frac{Sc}{2\alpha^2}\right]}{H\left[C_1, D+1, (d-1)\frac{Sc}{2\alpha^2}\right]}, \tag{39}$$

2.4 Uniform Mass Flux Case

Define the transformation for Eq. (4) as, $h(\eta) = \frac{C-C_\infty}{\frac{m_w}{D}\sqrt{v}}$, with following B.Cs,

$$\text{at } y = 0 \ , \ -D\frac{\partial C}{\partial y} = \frac{m_w}{\sqrt{(1-\gamma t)}}, \tag{40}$$
$$\text{as } y \to \infty \ , \ C \to C_\infty$$

Use Eq. (40) in Eq. (4) for $\gamma = -1$ will give,

$$h_{\eta\eta} - \frac{Sc}{2}\left[V_C - \frac{1-d}{\alpha} + \frac{1-d}{\alpha}Exp(-\alpha\eta)\right]h_\eta - \frac{1}{2}Sc\beta h = 0, \tag{41}$$

With B.Cs,

$$h_\eta(0) = -1 \ , \ h(\infty) = 0, \tag{42}$$

The Eq. (41) is similar to Eq. (31b) upto their general solution,

$$h(\eta) = {C_1}^1(1-d)^{C_1}\left(\frac{Sc}{2\alpha^2}\right)^{C_1} Exp(-C_1\alpha\eta)H\left[C_1, D+1, (d-1)\frac{Sc}{2\alpha^2}Exp(-\alpha\eta)\right], \tag{43}$$

On using B.Cs as in Eq. (42), Eq. (43) will imply.

$$h(\eta)=\frac{Exp(-C_1\alpha\eta)H\left[C_1,D+1,(d-1)\frac{Sc}{2\alpha^2}Exp(-\alpha\eta)\right]}{\alpha C_1\left\{H\left[C_1,D+1,(d-1)\frac{Sc}{2\alpha^2}\right]+\frac{1-d}{D+1}\frac{Sc}{2\alpha^2}H\left[C_1+1,D+2,(d-1)\frac{Sc}{2\alpha^2}\right]\right\}}, \tag{44}$$

2.5 General Power Law Wall Concentration

In the current section we examined the general condition by assuming the wall concentration with a power law dependence on both time and distance as $C_w=C_\infty+C_{ref}x^n(1-\gamma t)^m$, where$n,m\in R$. Now define the dimensionless concentration as follows:

$$C=C_\infty+(C_w-C_\infty)x^n(1-\gamma t)^m\Phi(\eta),\quad\text{and}\quad\Phi(\eta)=\frac{C-C_\infty}{C_w-C_\infty}, \tag{45}$$

by applying this new definition in Eq. (4) to obtain the following ODE for $\gamma=-1$,

$$\Phi_{\eta\eta}+Sc\left(af+\frac{1}{2}\eta\right)\Phi_\eta-Sc\left(anf_\eta+m-a\beta\right)\Phi=0, \tag{46}$$

With the following B.Cs,

$$\Phi(0)=1,\quad\Phi(\infty)=0. \tag{47}$$

For $a=-1/2$ and using Eqs. (28)–(30), Eq. (46) will reduce to,

$$\begin{aligned}\Phi_{\eta\eta}+Sc\left(\delta\alpha+\frac{1}{2}Da^{-1}+\frac{2}{\alpha}+\frac{(d-1)}{2\alpha}Exp[-\alpha\eta]\right)\Phi_\eta\\+Sc\left(\frac{n}{2}[1+(d-1)Exp[-\alpha\eta]]-m-\frac{\beta}{2}\right)\Phi=0\end{aligned}, \tag{48}$$

By introducing new variable $\xi=(d-1)\frac{Sc}{2\alpha^2}Exp(-\alpha\eta)$ in Eq. (48) to obtain,

$$\xi\frac{\partial^2\Phi}{\partial\xi^2}+(1-A_1-\xi)\frac{\partial\Phi}{\partial\xi}+\left(\frac{A_2}{\xi}+n\right)\Phi=0, \tag{49}$$

where, $A_1=Sc\left(\delta+\frac{2}{\alpha^2}+\frac{Da^{-1}}{2\alpha}\right)$, $A_2=\frac{1}{\alpha^2}Sc\left(\frac{n}{2}-m-\frac{\beta}{2}\right)$.

And the B.Cs will reduce to,

$$\Phi\left(\frac{Sc(\alpha-1)}{2\alpha^2}\right)=1,\quad\Phi(0)=0. \tag{50}$$

Now define $\Phi(\xi)=\xi^k\psi(\xi)$ in Eq. (49) to convert it into following expression,

$$\xi\frac{\partial^2\psi}{\partial\xi^2}+(\Gamma_1-\xi)\frac{\partial\psi}{\partial\xi}-(k-n)\psi=0, \tag{51}$$

Here $\Gamma = 1 + 2k - A_1$, and expression for k is given by,

$$k = \frac{A_1 \pm \sqrt{{A_1}^2 - 4A_2}}{2}, \quad \text{with} \quad \frac{Sc}{4\alpha^2}\left(2\delta\alpha^2 + 4 + \alpha Da^{-1}\right)^2 \geq 2n - 4m - 2\Gamma, \tag{52}$$

Eq. (51) is the standard form of hypergeometric differential equation and its solution will be in the form of,

$$\psi(\xi) = C_1 M(k - n, \Gamma, \xi), \tag{53}$$

It gives the solution of Eq. (49) in the form, $\phi(\xi) = C_1 \xi^k M(k - n, \Gamma, \xi)$, therefore the solution of Eq. (48) with B.Cs as in Eq. (47) is obtained as,

$$\Phi(\eta) = \frac{Exp(-\alpha k\eta) M\left[k - n,\ \Gamma,\ (d-1)\frac{Sc}{2\alpha^2} Exp(-\alpha\eta)\right]}{M\left[k - n,\ \Gamma,\ (d-1)\frac{Sc}{2\alpha^2}\right]}, \tag{54}$$

And the wall mass flux is,

$$-\Phi_\eta(0) = \alpha k + \frac{Sc(d-1)(k-n)}{2\Gamma\alpha} \frac{M\left[1 + k - n,\ \Gamma + 1,\ (d-1)\frac{Sc}{2\alpha^2}\right]}{M\left[k - n,\ \Gamma,\ (d-1)\frac{Sc}{2\alpha^2}\right]}. \tag{55}$$

2.6 General Power-Law Mass Flux

In this section, the general condition is assumed with the wall concentration by a power law dependence on both time and distance $-D\frac{\partial C}{\partial y} = m_w x^n (1 - \gamma t)^{m - \frac{1}{2}}$, where $n, m \in R$. Now define the dimensionless concentration as follows:

$$C = C_\infty + \frac{m_w}{D}\sqrt{\nu} x^n (1 - \gamma t)^m H(\eta), \tag{56}$$

Use Eq. (56) in Eq. (4) for $\gamma = -1$ will give,

$$H_{\eta\eta} + Sc\left(af + \frac{1}{2}\eta\right)H_\eta - Sc\left(anf_\eta + m - a\beta\right)H = 0. \tag{57}$$

With B.Cs as,

$$H_\eta(0) = -1, \quad H(\infty) = 0, \tag{58}$$

Eq. (57) is the same as Eq. (46), therefore their solutions are similar. We can obtain the solution of Eq. (57) as,

$$H(\eta) = C_1 \left[(d-1)\frac{Sc}{2\alpha^2}\right]^k Exp(-\alpha k\eta) M\left[k - n,\ \Gamma,\ (d-1)\frac{Sc}{2\alpha^2} Exp(-\alpha\eta)\right], \tag{59}$$

On applying B.C as in Eq. (58) to Eq. (59), we obtain the solution of Eq. (57) as follows:

$$H(\eta) = \frac{2\Gamma\alpha Exp(-\alpha k\eta)M\left[k-n,\ \Gamma,\ (d-1)\frac{Sc}{2\alpha^2}Exp(-\alpha\eta)\right]}{2\alpha^2 k\Gamma M\left[k-n,\ \Gamma,\ (d-1)\frac{Sc}{2\alpha^2}\right] + Sc(k-n)(d-1)M\left[k-n+1,\ \Gamma+1,\ (d-1)\frac{Sc}{2\alpha^2}\right]}, \quad (60)$$

The current work with nanoparticles dispersed in the base fluid is well agreement with the investigation of Fang et al. [9] in the absence of nanoparticles, porous media, stagnation point parameter and chemical reaction parameter.

3 Results and Discussion

The examination of unsteady stagnation point flow over porous media with mass transpiration and mass transfer with chemical reaction for $Cu\text{-}Al_2O_3/H_2O$ hybrid nanofluid is carried out to observe several results. The momentum and mass transfer problem are combined to form the system of PDEs (1) to (4), then the system is converted into system of ODEs (11) to (12) via similarity transformations. Then the governing ODEs are solved analytically to obtain the solution for velocity and concentration profiles in exponential and hypergeometric forms. Four different cases are considered for the concentration profile as constant wall concentration, uniform mass flux, general power law wall concentration and general power law mass flux. The effect of different physical parameters such as Darcy number (Da^{-1}), mass transpiration parameter (V_C), stretching/shrinking parameter (d), chemical reaction parameter (β), Schmidt number (Sc) on velocity and concentration profile is examined under different situations. These effects are observed with the help of graphical representation of physically interested parameters for the solid volume fraction of Al_2O_3 nanoparticle (φ_1) which is taken as 0.1 and that of Cu nanoparticle (φ_2) is fixed at 0.04.

Fig. 2 demonstrates the solution domain α *versus* d for different values of V_C. It can be observed that, as the mass transpiration decreases from suction to injection, the solution domain will expand for negative values of d.

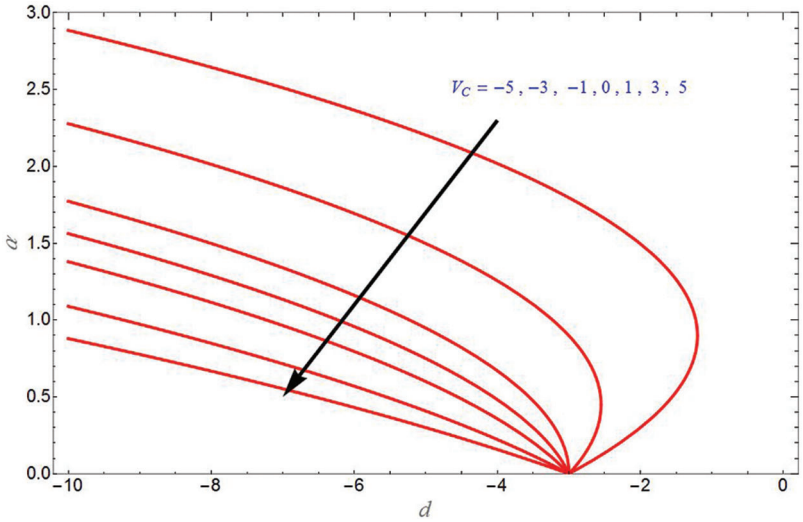

Figure 2: α *vs.* stretching/shrinking parameter d for different values of mass transpiration parameter V_C

Fig. 3 depicts the transverse velocity due to stretching sheet and different values of V_C in Fig. 3a. It shows that transverse velocity increases with increase in V_C. Fig. 3b demonstrates the transverse velocity for different values of Da^{-1} and it will increase with increase in Da^{-1}.

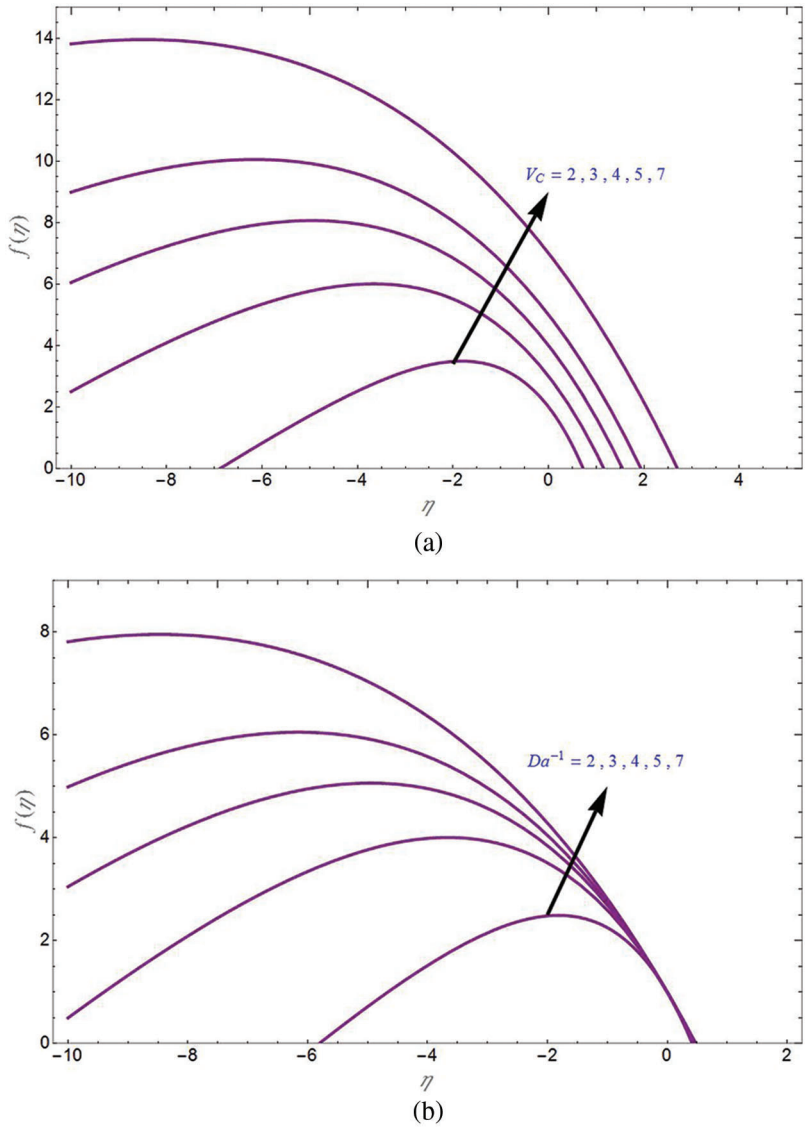

Figure 3: Transverse velocity $f(\eta)$ for different values of V_C in (a) and Da^{-1} in (b)

Fig. 4a is the plot for axial velocity due to shrinking sheet $(d = -4)$ with various values of V_C. In this situation, axial velocity is negative and it is decreases with increase in mass transpiration from injection to suction. Furthermore, Fig. 4b is the plot for axial velocity due to stretching sheet $(d = 2)$ with various values of injection parameter. In this situation axial velocity is positive and it is increased with increase in injection parameter. Fig. 5 is depicted for axial velocity due to shrinking sheet $(d = -4)$ with various values of Da^{-1}. In this condition axial velocity is negative and it is decreased with increase in Da^{-1} for both suction and

injection cases. Fig. 6 investigates the axial velocity due to shrinking sheet with various values of shrinking sheet parameter. As the shrinking sheet parameter increases, the axial velocity will decrease in both suction and injection cases.

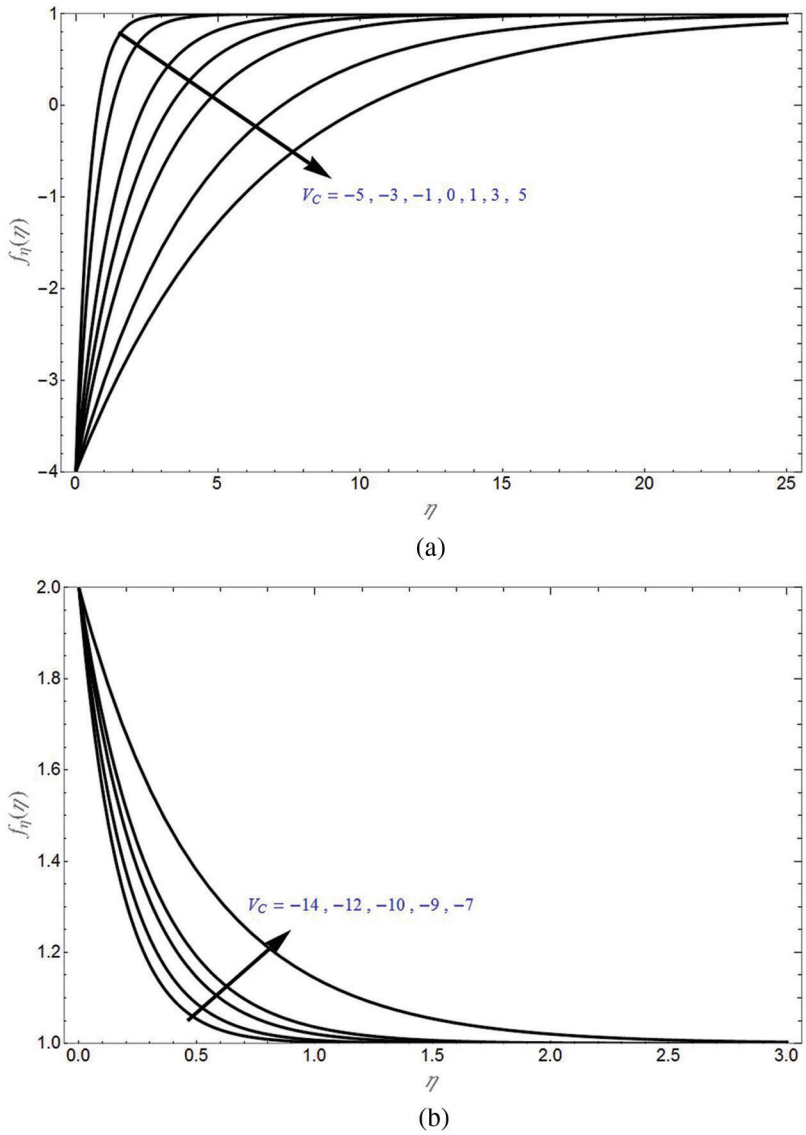

Figure 4: Axial velocity $f_\eta(\eta)$ for different values of V_C for shrinking sheet in (a) and stretching sheet in (b)

The concentration profiles for different values of shrinking sheet parameter are demonstrated in Fig. 7 for suction and non-permeability cases in Figs. 7a and 7b, respectively. It can be seen that $\phi(\eta)$ will decrease with increase in shrinking sheet parameter. Initially, $\phi(\eta)$ will decrease upto certain value of η and then become constant to 0.

The concentration profile for different values of β is demonstrated in Fig. 8 for non-permeability and injection case in Figs. 8a and 8b, respectively. It can be seen that $\phi(\eta)$ will decrease with increase in β.

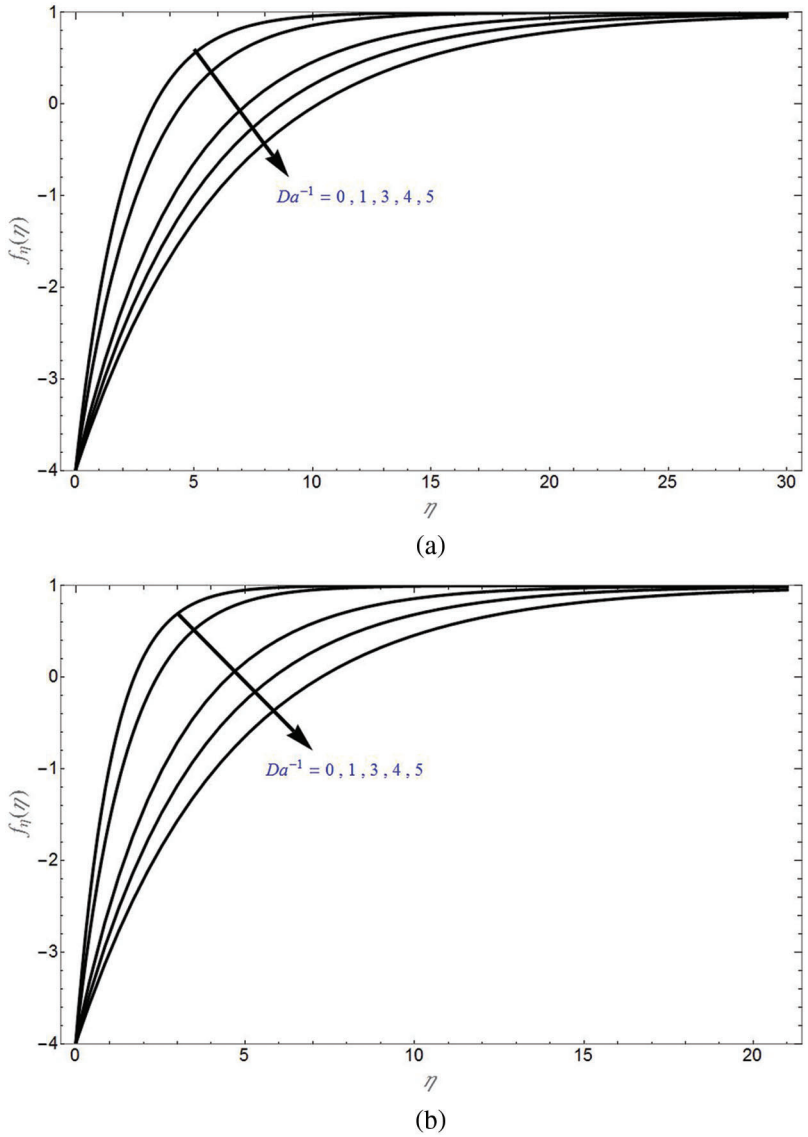

Figure 5: Axial velocity $f_\eta(\eta)$ for different values of Da^{-1} due to shrinking sheet for suction case $(V_C = 1)$ in (a) and injection case $(V_C = -1)$ in (b)

The concentration profile for different values of mass transpiration parameter due to shrinking sheet $(d = -4)$ is demonstrated in Fig. 9. It can be seen that $\phi(\eta)$ will decrease with increase in mass transpiration from injection to suction.

The concentration profile of mass flux case for different values of shrinking sheet parameter is demonstrated in Fig. 10 for suction, non-permeability and injection cases, respectively in Figs. 10a–10c. It can be seen that $h(\eta)$ will decrease with increase in shrinking sheet parameter. Initially, $h(\eta)$ will decrease upto certain value of η and then become constant to 0. On compare, injection case has more mass transfer than non-permeable case and non-permeable case has more mass transfer than suction case and the difference is very less in this case.

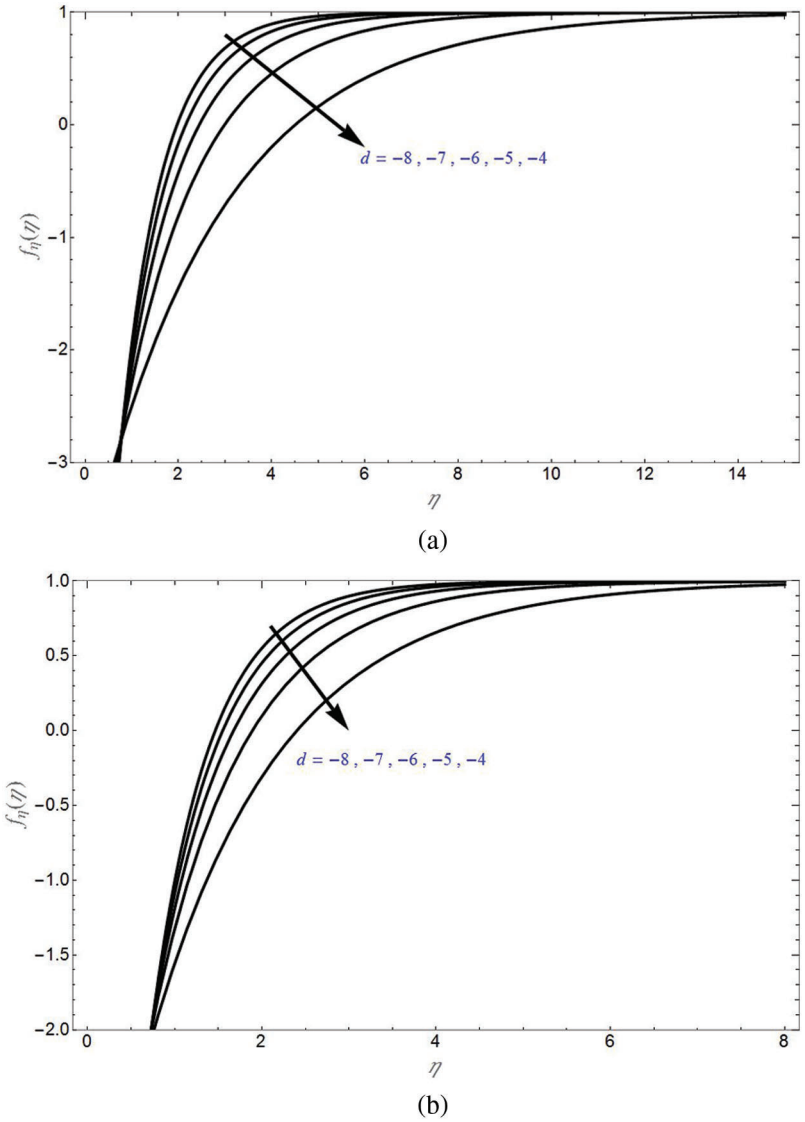

Figure 6: Axial velocity $f_\eta(\eta)$ for different values of shrinking sheet parameter for suction case $(V_C = 1)$ in (a) and injection case $(V_C = -1)$ in (b)

The concentration profile of mass flux case for different values of β due to shrinking sheet $(d = -4)$ is demonstrated in Fig. 11 for suction, non-permeability and injection case in Figs. 11a–11c, respectively. It can be seen that $h(\eta)$ will decrease with increase in β. On compare, injection case has more mass transfer than non-permeable case and non-permeable case has more mass transfer than suction case and the difference is greater in this case.

The concentration profile of mass flux case for different values of mass transpiration parameter due to shrinking sheet $(d = -4)$ is demonstrated in Fig. 12. It can be seen that $h(\eta)$ will decrease with increase in mass transpiration from injection to suction. Injection case has more transfer than suction case.

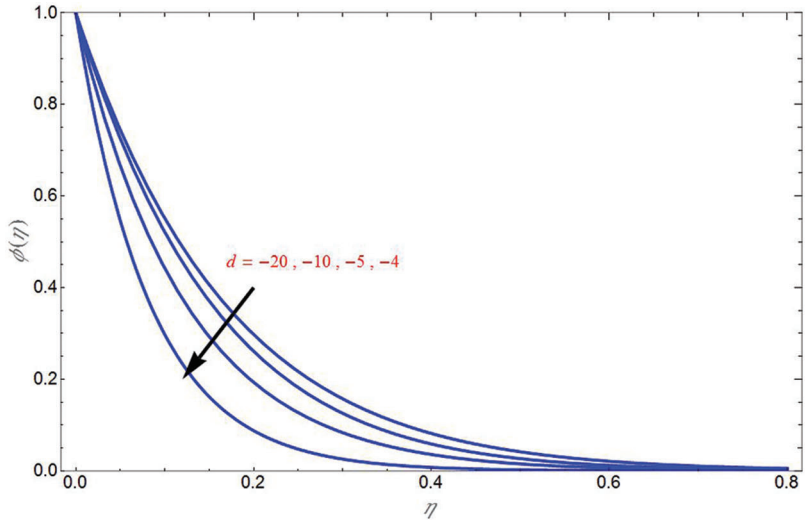

(a)

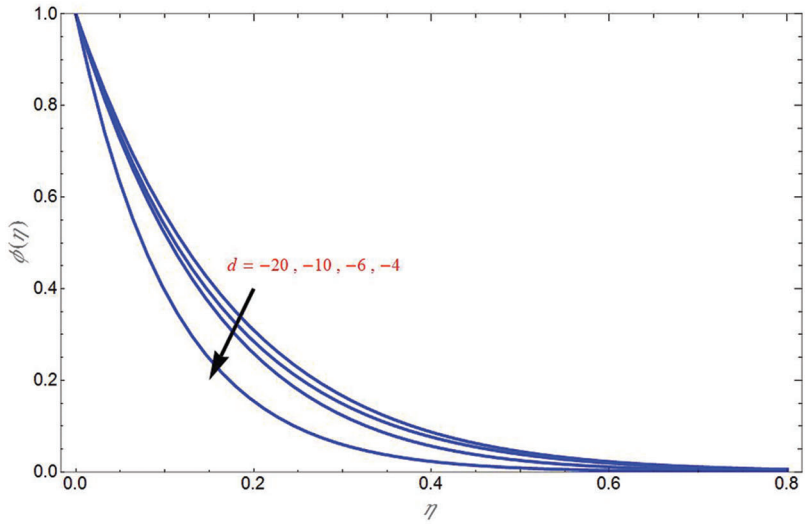

(b)

Figure 7: Concentration profile $\phi(\eta)$ for different values of shrinking sheet parameter for suction case $(V_C = 1)$ in (a) and non-permeability case $(V_C = 0)$ in (b)

The concentration profile of mass flux case for different values of *Sc* due to shrinking sheet $(d = -4)$ is demonstrated in Fig. 13 for suction, non-permeability and injection case in Figs. 13a–13c, respectively. It can be seen that $h(\eta)$ will decrease with increase in *Sc*. By a comparison study, it can be found that injection case has more mass transfer than non-permeable case and non-permeable case has more mass transfer than suction case and the difference is more in this case also.

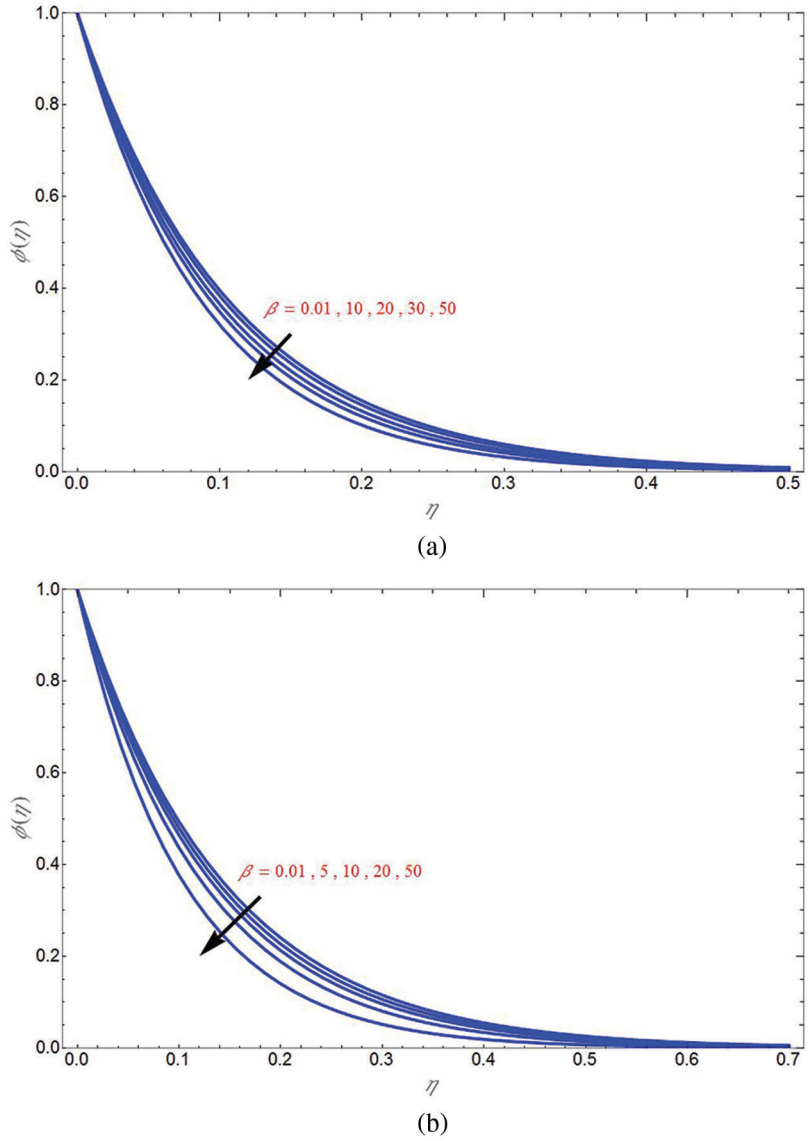

Figure 8: Concentration profile $\phi(\eta)$ for different values of β due to shrinking sheet parameter for non-permeability case $(V_C = 0)$ in (a) and injection case $(V_C = -1)$ in (b)

The concentration profile of mass flux case for different values of Da^{-1} due to shrinking sheet $(d = -4)$ is demonstrated in Fig. 14 for suction, non-permeability and injection case respectively in Figs. 14a–14c. It can be seen that $h(\eta)$ will decrease with increase in Da^{-1}.

Fig. 15 shows the general power law wall concentration profile for different values of shrinking sheet parameter for suction, non-permeability and injection cases in Figs. 15a–15c, respectively. It can be seen that $\Phi(\eta)$ will increase with increase in shrinking sheet parameter. Initially $\Phi(\eta)$ decreases upto certain value of η and then become constant to 0.

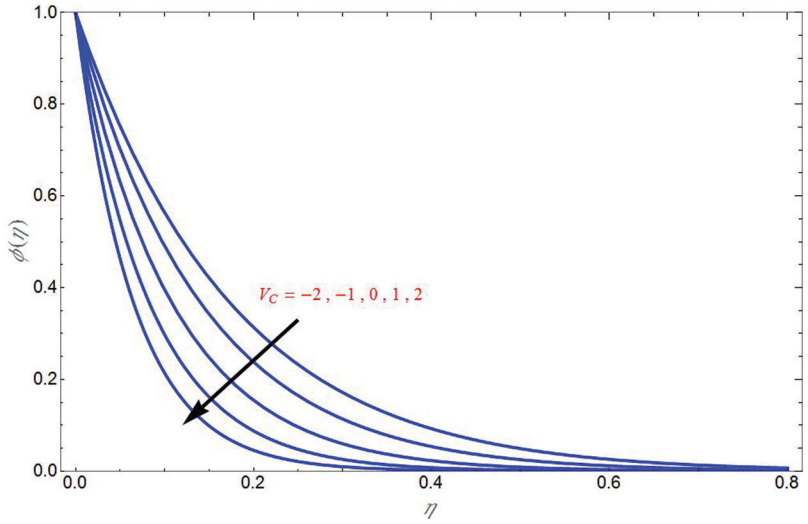

Figure 9: Concentration profile $\phi(\eta)$ for different values of suction/injection parameter due to shrinking sheet parameter

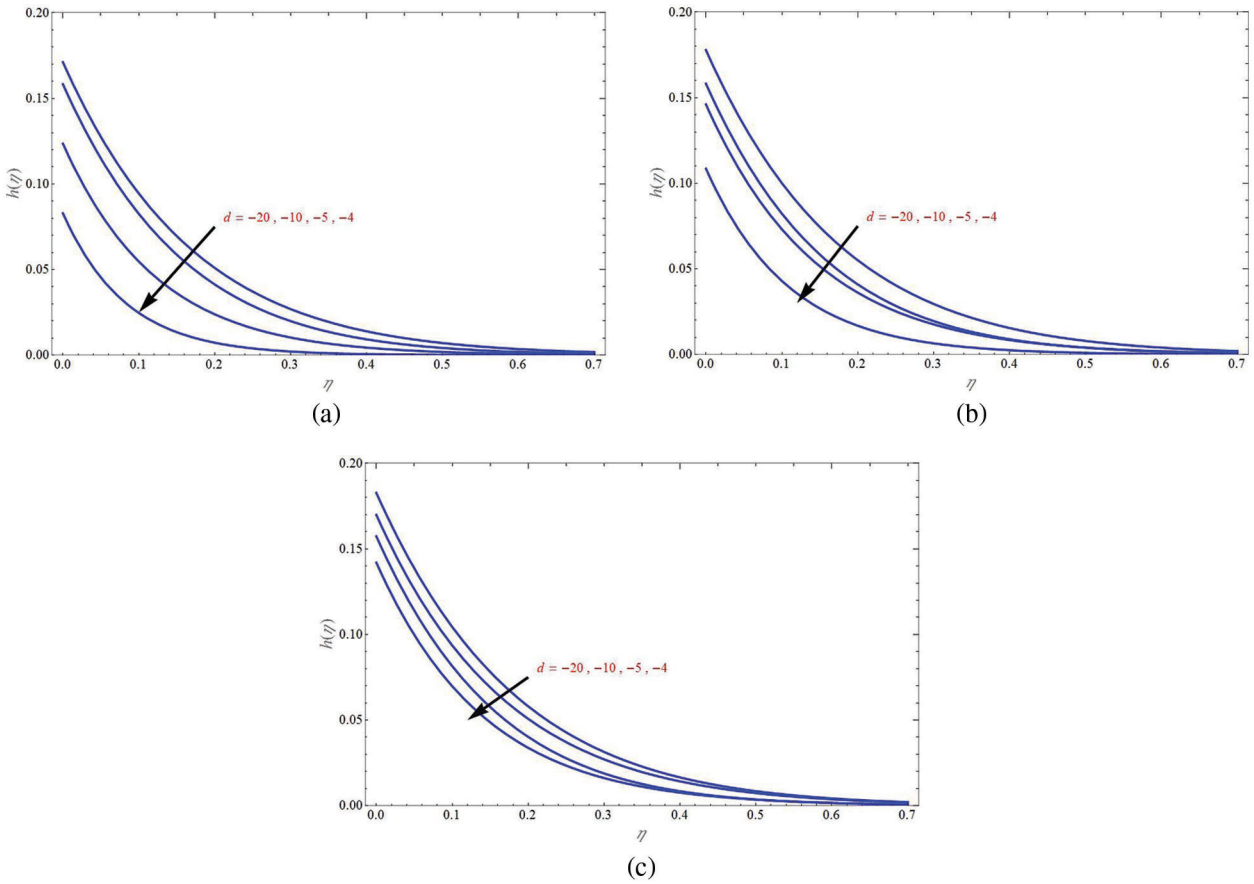

Figure 10: Concentration profile $h(\eta)$ of mass flux case for different values of shrinking sheet parameter for suction case $(V_C = 1)$ in (a) no-permeability case $(V_C = 0)$ in (b) and injection case $(V_C = -1)$ in (c)

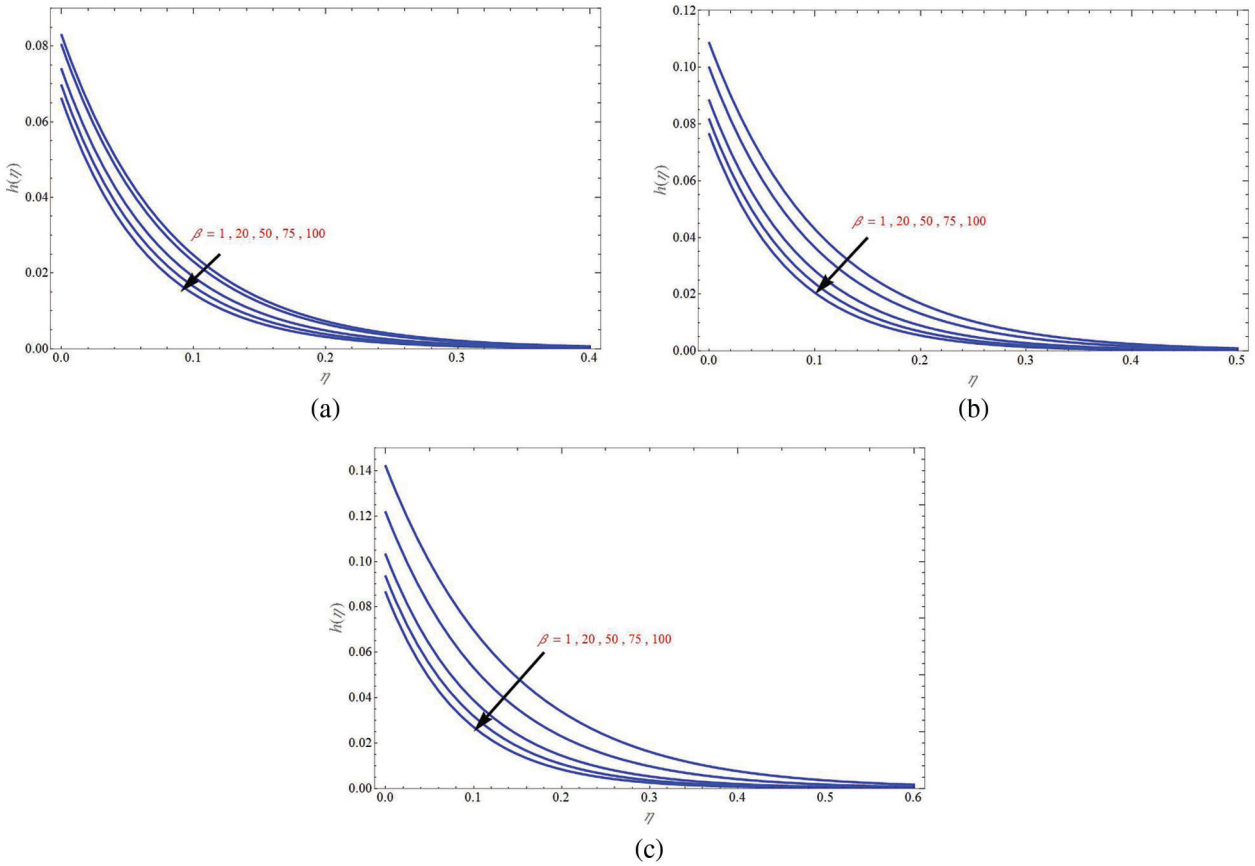

Figure 11: Concentration profile $h(\eta)$ of mass flux case for different values of β due to shrinking sheet for suction case $(V_C = 1)$ in (a) non-permeability case $(V_C = 0)$ in (b) and injection case $(V_C = -1)$ in (c)

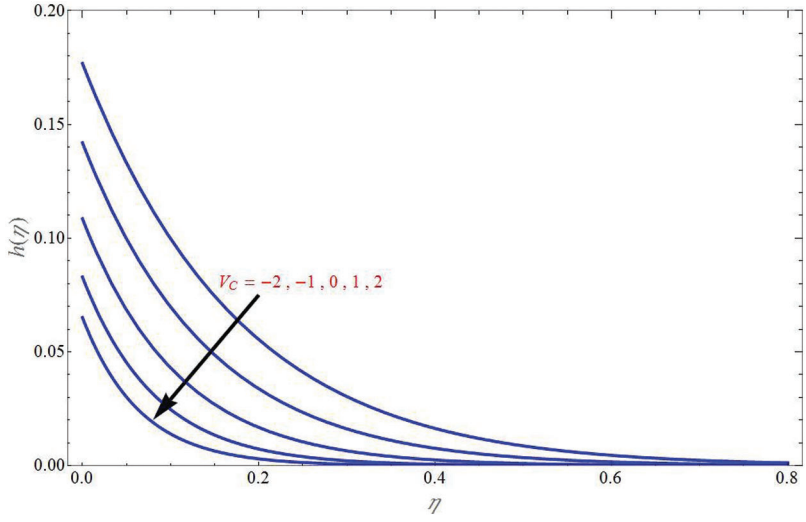

Figure 12: Concentration profile $h(\eta)$ of mass flux case for different values of V_C due to shrinking sheet

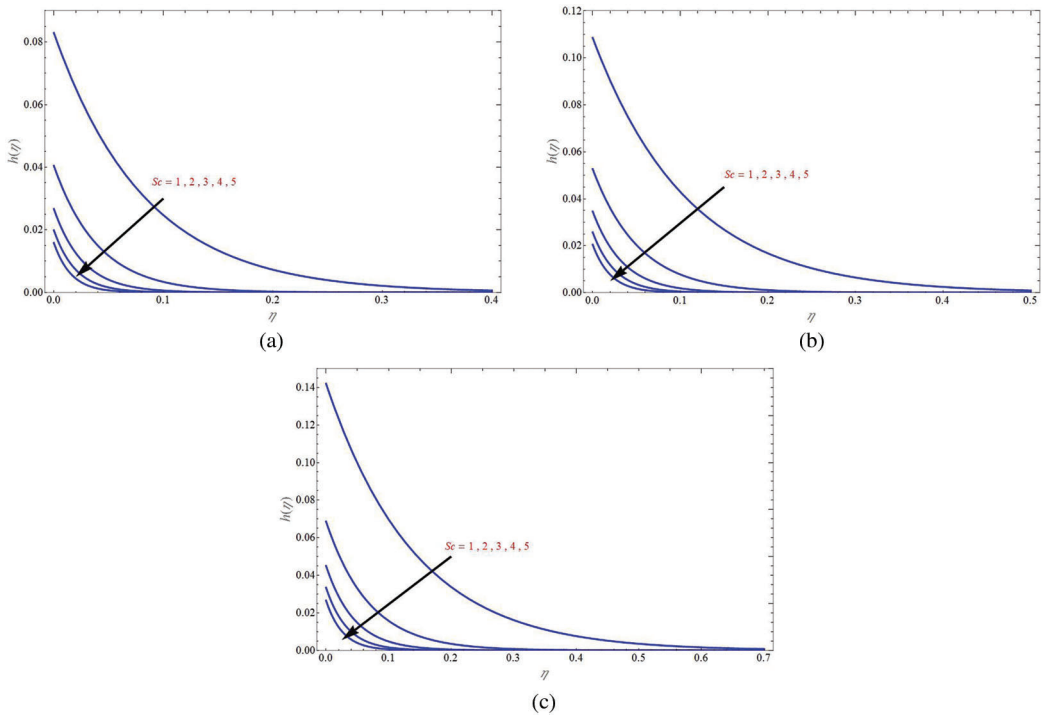

Figure 13: Concentration profile $h(\eta)$ of mass flux case for different values of Schmidt number (Sc) due to shrinking sheet for suction case $(V_C = 1)$ in (a) no-permeability case $(V_C = 0)$ in (b) and injection case $(V_C = -1)$ in (c)

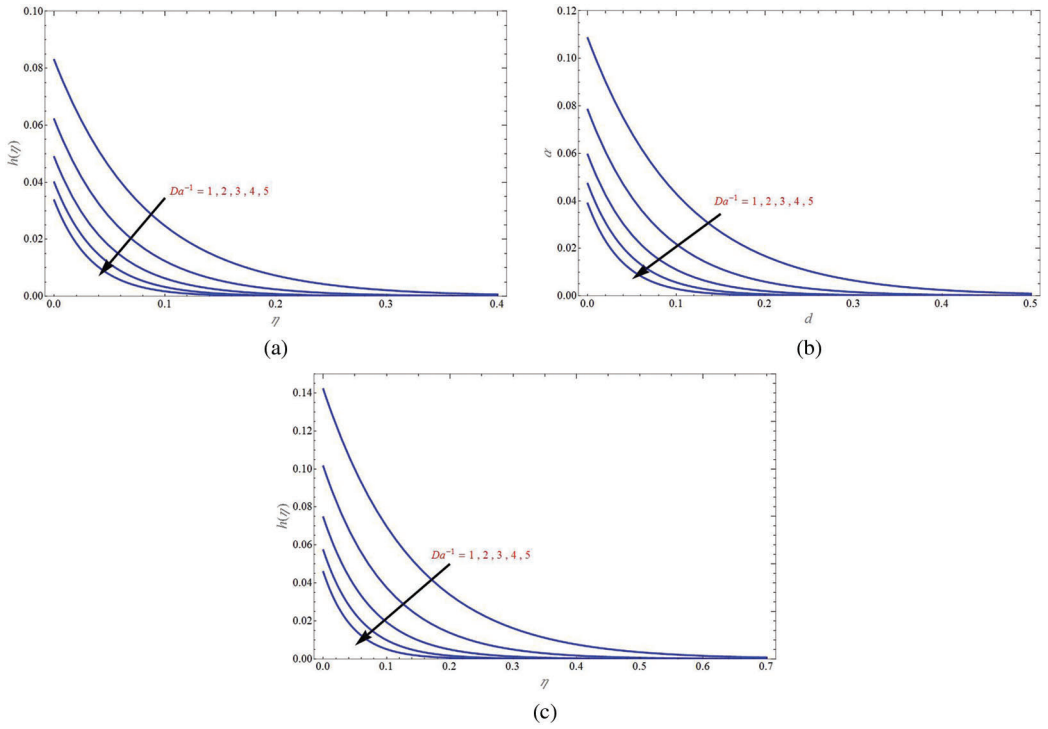

Figure 14: Concentration profile $h(\eta)$ of mass flux case for different values of Da^{-1} due to shrinking sheet for suction case $(V_C = 1)$ in (a) no-permeability case $(V_C = 0)$ in (b) and injection case $(V_C = -1)$ in (c)

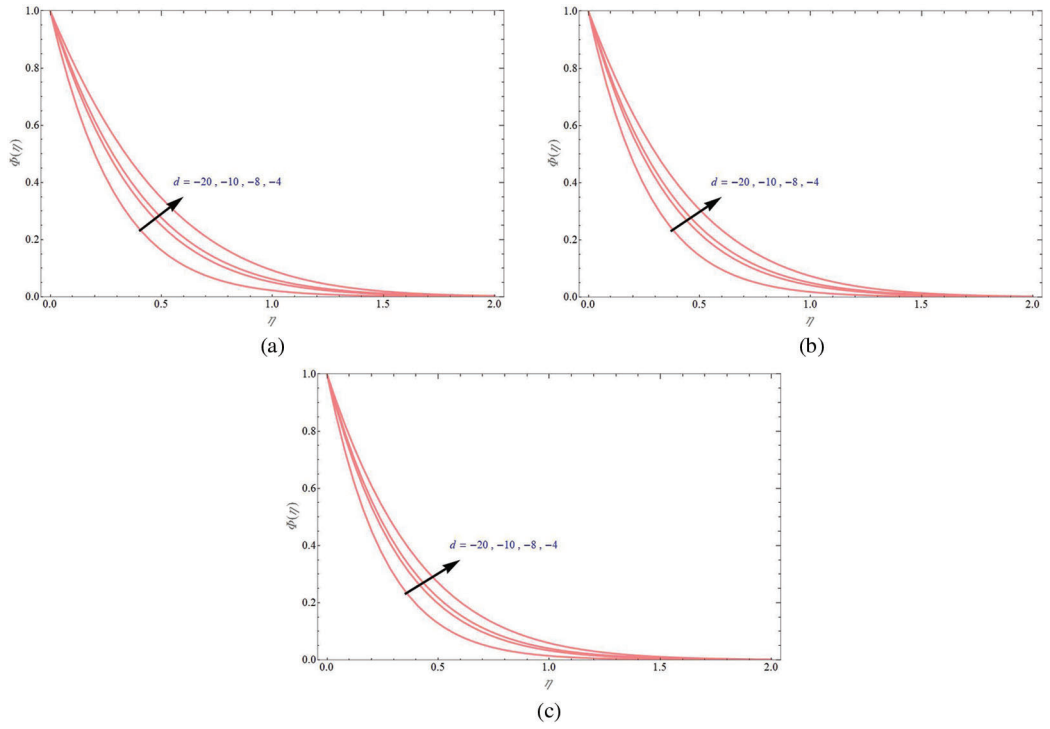

Figure 15: General power law wall concentration profile $\Phi(\eta)$ for different values of shrinking sheet parameter for suction case $(V_C = 1)$ in (a) no-permeability case $(V_C = 0)$ in (b) and injection case $(V_C = -1)$ in (c)

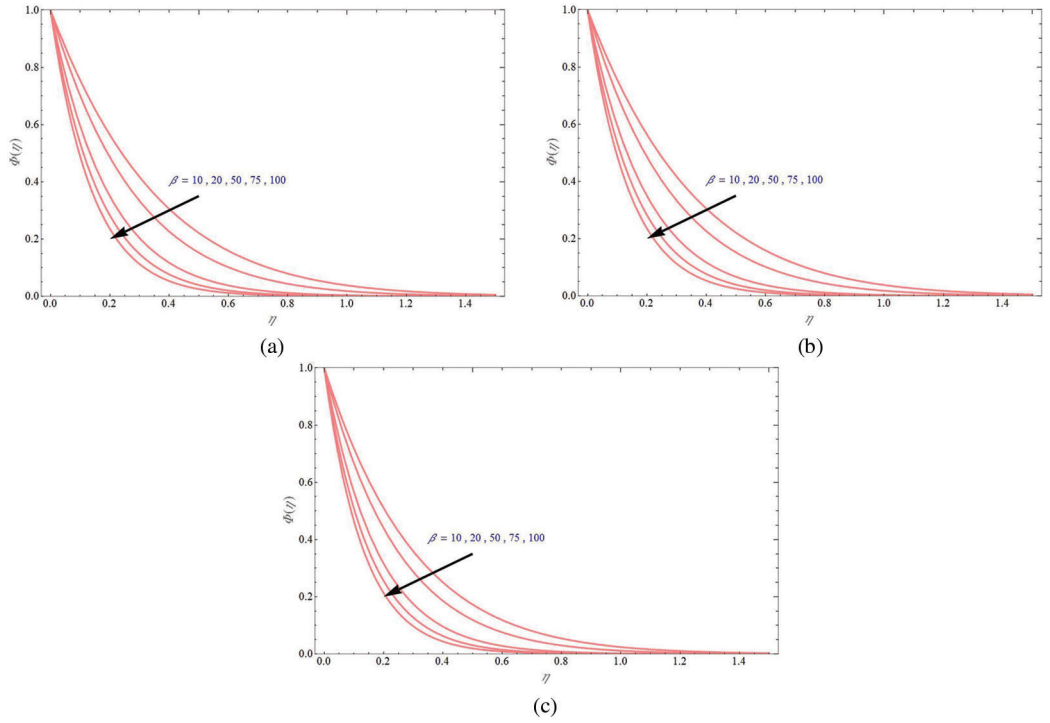

Figure 16: General power law wall concentration profile $\Phi(\eta)$ for different values of β due to shrinking sheet parameter for suction case $(V_C = 1)$ in (a) no-permeability case $(V_C = 0)$ in (b) and injection case $(V_C = -1)$ in (c)

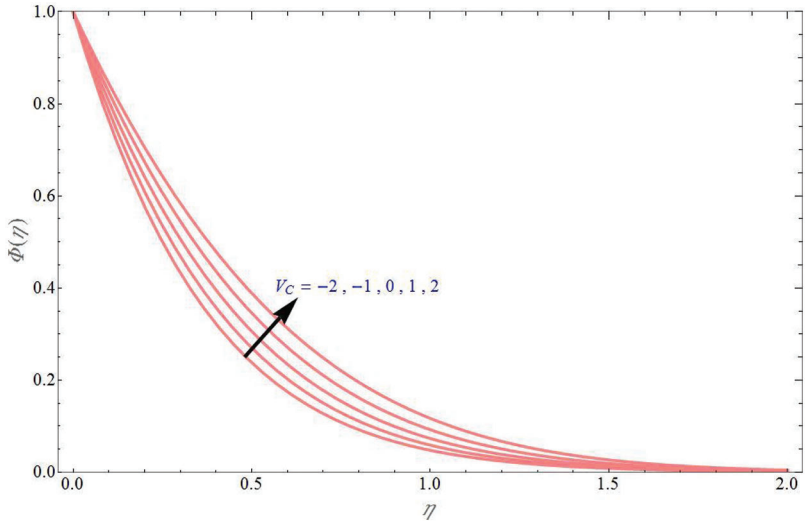

Figure 17: The general power law wall concentration profile $\Phi(\eta)$ for different values of V_C due to shrinking sheet

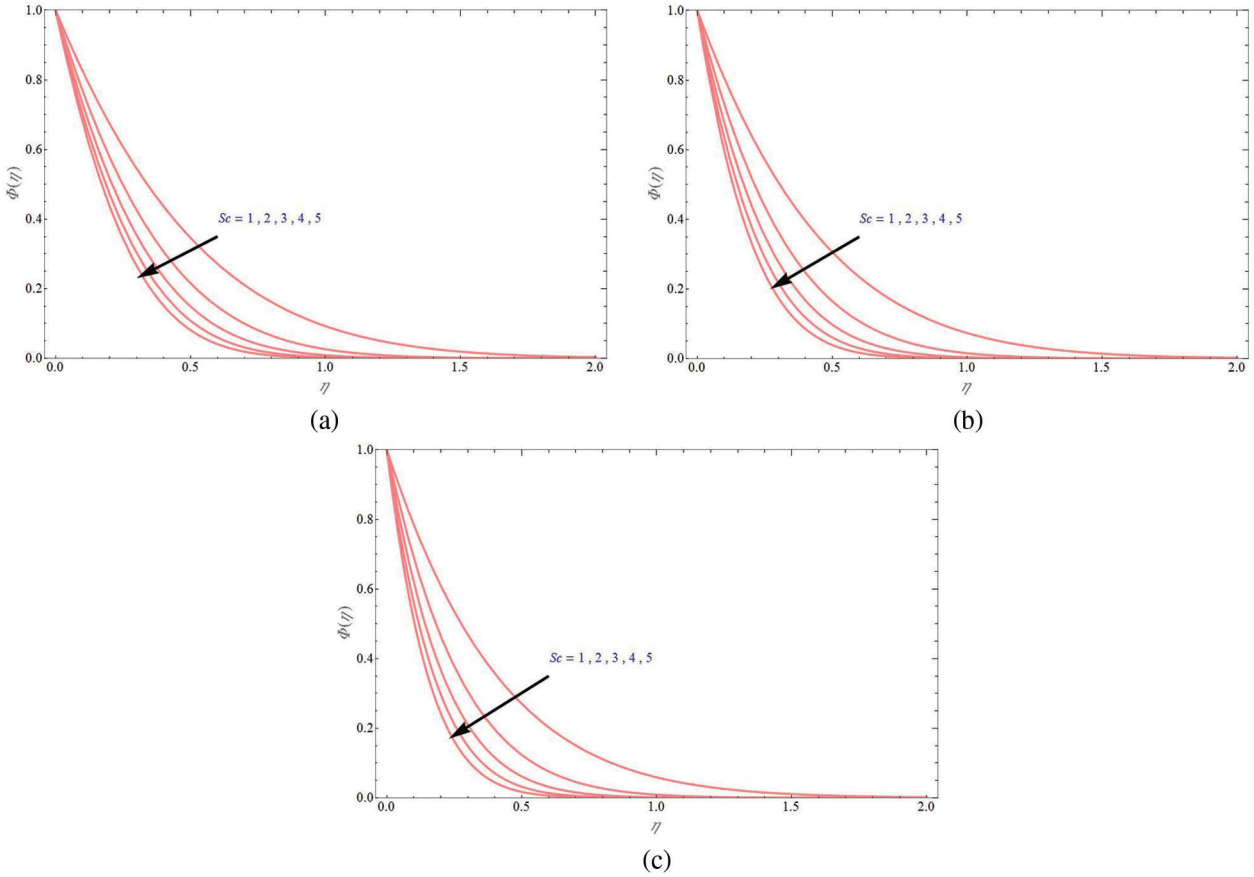

Figure 18: The general power law wall concentration profile $\Phi(\eta)$ for different values of Schmidt number (Sc) due to shrinking sheet for suction case $(V_C = 1)$ in (a) no-permeability case $(V_C = 0)$ in (b) and injection case $(V_C = -1)$ in (c)

Furthermore, Fig. 16 demonstrates the general power law wall concentration profile for different values of β due to shrinking sheet $(d = -4)$ for suction, non-permeability and injection case respectively in Figs. 16a–16c. It can be seen that $\Phi(\eta)$ will decrease with increase in β.

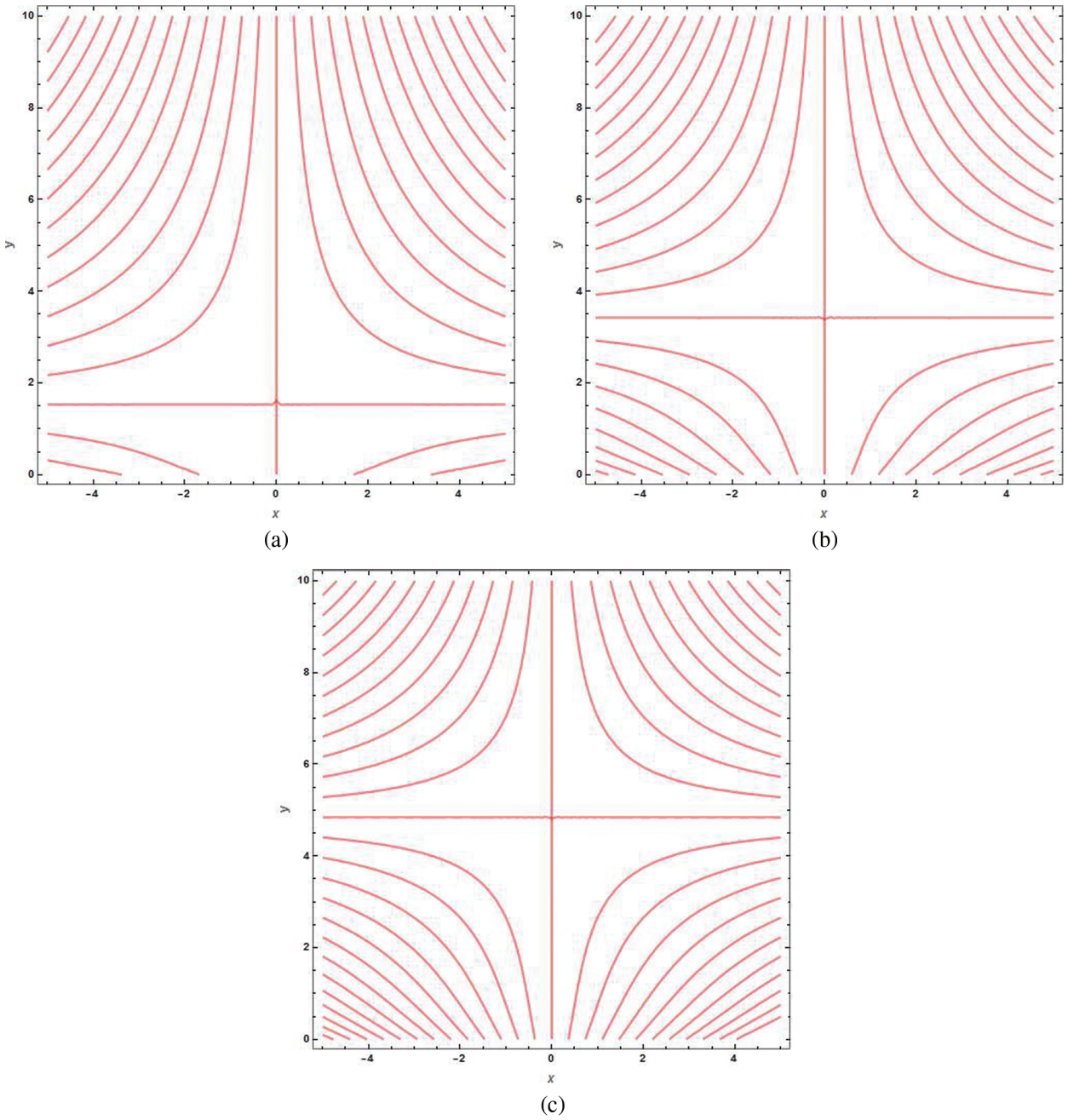

Figure 19: Stream line graphs for upper branch solution keeping $V_C = -6$, $d = -1$, $K = 1$, in (a) $t = 0.1$, in (b) $t = 0.5$ and in (c) $t = 1$

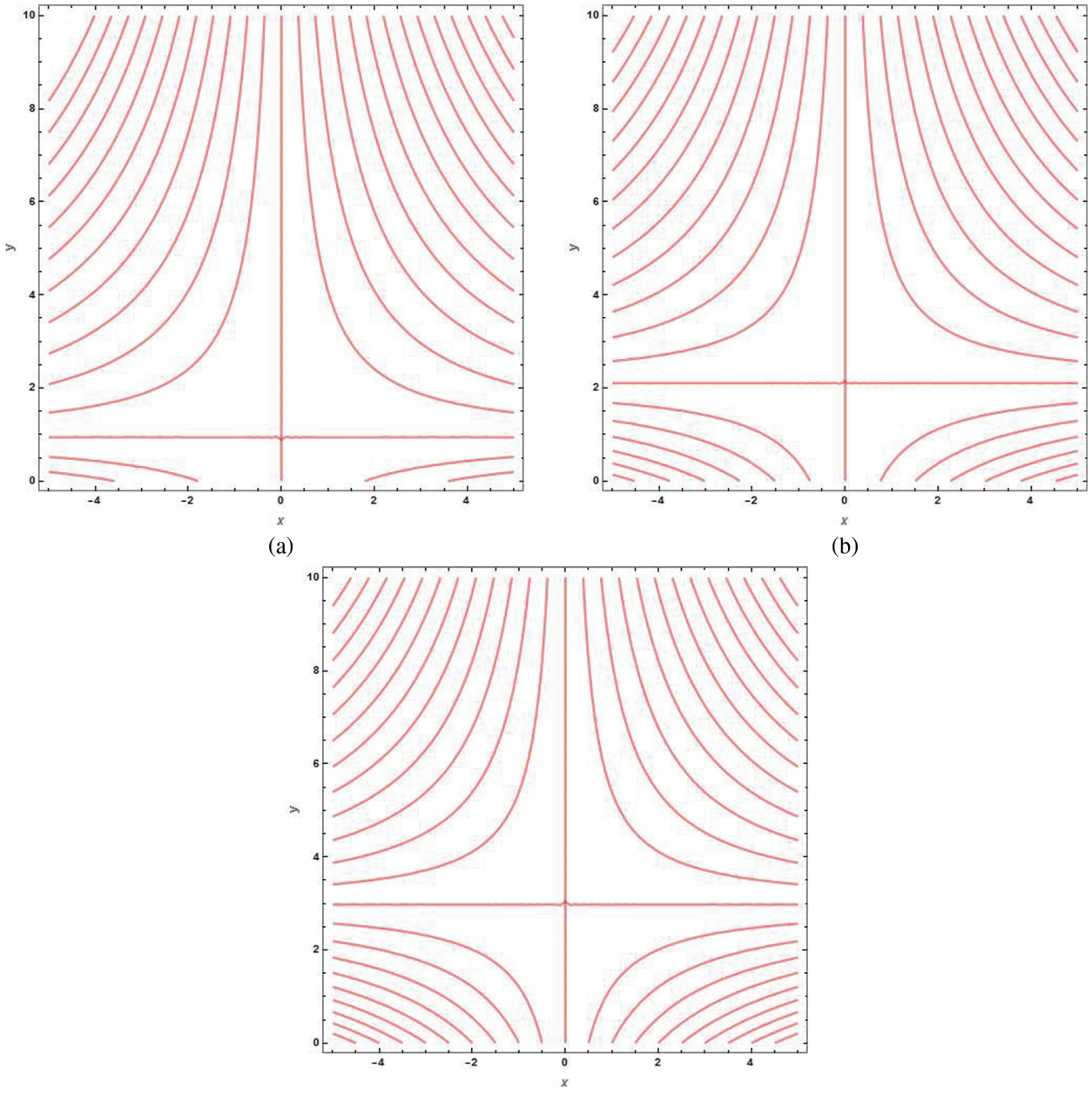

Figure 20: Stream line graphs for lower branch solution keeping $V_C = -6$, $d = -1$, $K = 1$, in (a) $t = 0.1$, in (b) $t = 0.5$ and in (c) $t = 1$

The general power law wall concentration profile for different values of mass transpiration parameter due to shrinking sheet $(d = -4)$ is demonstrated in Fig. 17. It can be seen that $\Phi(\eta)$ will increase with increase in mass transpiration from injection to suction and it seems that suction case has more transfer than injection case.

The general power law wall concentration profile for different values of Sc due to shrinking sheet $(d = -4)$ is demonstrated in Fig. 18 for suction, non-permeability and injection case respectively in Figs. 18a–18c. It can be seen that $\Phi(\eta)$ will decrease with increase in Sc.

Finally, Figs. 19 and 20 demonstrate the stream line graphs for upper branch solution and lower branch solution, respectively for some values of time $t = 0.1, 0.5, 1$. Stretching velocity of the wall is away from the origin since stream velocity is towards the origin. It can be seen that as the time increases, the stagnation point is moving away from the origin and towards the positive y direction.

4 Conclusion

The current work examined the unsteady stagnation point HNF flow over porous sheet with mass transpiration and mass transfer with chemical reaction. The momentum and mass transfer problem are solved analytically to obtain the solution for velocity and concentration profiles in exponential form and hypergeometric form respectively. The concentration profile is obtained for four different cases such as constant wall concentration, uniform mass flux, general power law wall concentration and general power law mass flux. The effect of different physical parameters like Darcy number (Da^{-1}), mass transpiration parameter (V_C), stretching/shrinking parameter (d), chemical reaction parameter (β), Schmidt number (Sc) on velocity and concentration profile is examined under different situations. The observations are as follows:

- The solution domain will expand as mass transpiration decreases for shrinking sheet case.
- Transverse velocity increases with increase in V_C and Da^{-1}.
- Axial velocity decreases with increase in mass transpiration and it decreases with increase in Da^{-1} for both suction and injection cases.
- The axial velocity will decrease as the shrinking sheet parameter increases both in suction and injection cases.
- Concentration profile $\phi(\eta)$ will decrease with increase in shrinking sheet parameter or chemical reaction parameter or mass transpiration.
- The concentration profile of mass flux case $h(\eta)$ will decrease with increase in shrinking sheet parameter, chemical reaction parameter, mass transpiration, Schmidt number or inverse Darcy number.
- Injection case had more mass transfer than suction case.
- The general power law wall concentration profile $\Phi(\eta)$ will increase with increase in shrinking sheet parameter or mass transpiration and it will decrease with increase in chemical reaction parameter or Schmidt number.

Acknowledgement: The author T. Anusha is thankful to Council of Scientific and Industrial Research (CSIR), New Delhi, India for financial support in the form of Junior Research Fellowship: File No. 09/1207(0003)/2020-EMR-I.

Funding Statement: The authors received no specific funding for this study.

Conflicts of Interest: The authors declare that they have no conflicts of interest to report regarding the present study.

References

1. Crane, L. J. (1970). Flow past a stretching plate. *Zeitschrift für angewandte Mathematik und Physik ZAMP, 21(4),* 645–647. DOI 10.1007/BF01587695.
2. Wang, C. Y. (1984). The three-dimensional flow due to a stretching flat surface. *Physics of Fluids, 27,* 1915–1917.

3. Aly, E. H., Pop, I. (2020). MHD flow and heat transfer near stagnation point over a stretching/shrinking surface with partial slip and viscous dissipation: Hybrid nanofluid versus nanofluid. *Powder Technology, 367(1),* 192–205. DOI 10.1016/j.powtec.2020.03.030.
4. Aly, E. H., Pop, I. M. (2019). MHD flow and heat transfer over a permeable stretching/shrinking sheet in a hybrid nanofluid with a convective boundary condition. *International Journal of Numerical Methods for Heat and Fluid Flow, 29(9),* 3012–3038. DOI 10.1108/HFF-12-2018-0794.
5. Turkyilmazoglu, M. (2011). Multiple solutions of heat and mass transfer of MHD slip flow for the viscoelastic fluid over a stretching sheet. *International Journal of Thermal Sciences, 50(11),* 2264–2276. DOI 10.1016/j.ijthermalsci.2011.05.014.
6. Anusha, T., Huang, H. N., Mahabaleshwar, U. S. (2021). Two dimensional unsteady stagnation point flow of Casson hybrid nanofluid over a permeable flat surface and heat transfer analysis with radiation. *Journal of Taiwan Institute of Chemical Engineers, 127(8),* 79–91. DOI 10.1016/j.jtice.2021.08.014.
7. Anusha, T., Mahabaleshwar, U. S., Sheikhnejad, Y. (2021). An MHD of nanofluid flow over a porous stretching/shrinking plate with mass transpiration and Brinkman ratio. *Transport in Porous Media, 142(1–20),* 333–352. DOI 10.1007/s11242-021-01695-y.
8. Mahabaleshwar, U. S., Anusha, T., Hatami, M. (2021). The MHD Newtonian hybrid nanofluid flow and mass transfer analysis due to super-linear stretching sheet embedded in porous medium. *Scientific Reports, 11(1),* 1–17. DOI 10.1038/s41598-021-01902-2.
9. Fang, T. G., Wang, F. J. (2020). Momentum and heat transfer of a special case of the unsteady stagnation point flow. *Applied Mathematics and Mechanics, 41(1),* 51–82. DOI 10.1007/s10483-020-2556-9.
10. Mahabaleshwar, U. S., Sneha, K. N., Huang, H. N. (2021). An effect of MHD and radiation on CNTS-water based nanofluid due to a stretching sheet in a Newtonian fluid. *Case Studies in Thermal Engineering, 28(2),* 101462. DOI 10.1016/j.csite.2021.101462.
11. Siddheshwar, P. G., Mahabaleshwar, U. S., Andersson, H. I. (2013). A new analytical procedure for solving the non-linear differential equation arising the stretching sheet problem. *International Journal of Applied Mechanics and Engineering, 18(3),* 955–964.
12. Suresh, S., Venkitaraj, K., Selvakumar, P., Chandrasekar, M. (2012). Effect of Al_2O_3–Cu/water hybrid nanofluid in heat transfer. *Experimental Thermal and Fluid Science, 38,* 54–60.
13. Suresh, S., Venkitaraj, K., Selvakumar, P., Chandrasekar, M. (2011). Synthesis of Al_2O_3–Cu/water hybrid nanofluids using two step method and its thermo physical properties. *Colloids and Surface A, 388,* 41–48.
14. Momin, G. G. (2013). Experimental investigation of mixed convection with water-Al_2O_3 & hybrid nanofluid in inclined tube for laminar flow. *International Journal of Scientific and Technology Research, 2,* 195–202.
15. Mallikarjun, P., Murthy, R. V., Mahabaleshwar, U. S., Lorenzini, G. (2019). Numerical study of mixed convective flow of a couple stress fluid in a vertical channel with first order chemical reaction and heat generation/absorption. *Mathematical Modelling of Engineering Problems, 6(2),* 175–182.
16. Mahabaleshwar, U. S., Vishalakshi, A. B., Azese, M. N. (2022). The role of Brinkman ratio on non-Newtonian fluid flow due to a porous shrinking/stretching sheet with heat transfer. *European Journal of Mechanics–B Fluids, 92,* 153–165.
17. Mahabaleshwar, U. S., Vishalakshi, A. B., Andersson, H. I. (2022). Hybrid nanofluid flow past a stretching/shrinking sheet with thermal radiation and mass transpiration. *Chinese Journal of Physics, 75,* 152–168.
18. Nakhchi, M. E., Hatami, M., Rahmati, M. (2021). Effects of CuO nano powder on performance improvement and entropy production of double-pipe heat exchanger with innovative perforated turbulators. *Advanced Powder Technology, 32,* 3063–3074.
19. Nakhchi, M. E., Esfahani, J. A. (2021). Numerical investigation of turbulent CuO-water nanofluid inside heat exchanger enhanced with double V-cut twisted tapes. *Journal of Thermal Analysis and Calorimetry, 145,* 2535–2545.
20. Zainal, N. A., Nazar, R., Naganthran, K., Pop, I. M. (2020). Stability analysis of MHD hybrid nanofluid flow over a stretching/shrinking sheet with quadratic velocity. *Alexandria Engineering Journal, 60,* 915–926.

21. Khan, U., Shafiq, A., Zaib, A., Baleanu, D. (2020). Hybrid nanofluid on mixed convective radiative flow from an irregular variably thick moving surface with convex and concave effects. *Case Studies in Thermal Engineering, 21,* 100660.
22. Sarkar, J., Ghosh, P., Adil, A. (2015). A review on hybrid nanofluids: Recent research, development and applications. *Renewable and Sustainable Energy Reviews, 43,* 164–177.
23. Vishalakshi, A. B., Mahabaleshwar, U. S., Sarris, I. E. (2022). An MHD fluid flow over a porous stretching/shrinking sheet with slips and mass transpiration. *Micromachines, 13(1),* 116.
24. Sneha, K. N., Mahabaleshwar, U. S., Bennacer, R., Ganaoui, M. E. L. (2021). Darcy Brinkman equations for hybrid dusty nanofluid flow with heat transfer and mass transpiration. *Computation, 9(11),* 118.
25. Jalali, H., Abbassi, H. (2020). Analysis of the influence of viscosity and thermal conductivity on heat transfer by Al_2O_3-water nanofluid. *Fluid Dynamics and Materials Processing, 16(2),* 181–198. DOI 10.32604/fdmp.2020.07804.
26. Bhandari, A. (2019). Radiation and chemical reaction effects on nanofluid flow over a stretching sheet. *Fluid Dynamics and Materials Processing, 15(5),* 557–582. DOI 10.32604/fdmp.2019.04.